

Effect of Nearby Topography on Amplification of Seismic Motion in Topographic Irregularities: The Case Of a Hilly Site in Tehran



M. Khandan Bakavoli

University of Bojnord, Iran

E. Haghshenas

International Institute of Earthquake Engineering and Seismology, Iran

J. Bolouri Bazzaz

Ferdowsi University of Mashhad, Iran

M. Khandan Bakavoli

Central Tehran Branch, Islamic Azad University, Iran

SUMMARY:

This paper presents an experiment carried out in southern part of Tehran using nine Guralp CMG-6TD seismological stations that recorded 4 days of microtremor. The hill was a rocky site, instrumented in two perpendicular directions. The H/V and SSR technique have been used for evaluation of topographic site effect. The hill then was modelled numerically using a 2D finite-boundary element method code named HYBRID. The medium was assumed to have a linear elastic behaviour. The site was modelled both as single hill and in combination with adjacent topographies. The amplification patterns using 2D transfer function, in time and frequency domain, for each case, were determined. The amplification functions determined from the two different ways of modelling were compared with the ones derived from experimental studies. It is shown that effect of nearby topographies could justify some of the observed similarities and discrepancies between the curves derived from numerical and experimental studies.

Keywords: topography, amplification, hill

1. INTRODUCTION

There has been a lot of evidence of seismic amplification caused by topographic irregularities. Most studies have been focused on isolated ridges. Bard (1982) attributed such variations of seismic motion of topographic irregularities to focusing of seismic waves near the crest of the ridge due to interaction between incident and diffracted waves. Moreover, where the wavelength is comparable to horizontal width of a particular topographic structure, such as a mountain, amplification can be due to resonance of the whole topographic prominence with the incident seismic field.

Besides in some experimental studies, it is revealed that the observed amplification can be due to stratigraphy (Geli and Bard, 1988), presence of fractured rock and near surface weathering (Lebrun et al., 1999), low velocity layers (Grazier, 2009) or fault zones (Rovelli, 2002).

Among the first researches, Geli et al. (1988) investigated the seismic behaviour of 2D semi sinusoidal hills using Aki-Larner method. Three adjacent hills were subjected to incident SH waves. It was shown that amplification pattern of the isolated and combined hills were qualitatively the same but there were some discrepancies, quantitatively, between the results. In the current research the effect of nearby topography on the site response of the studied hill was investigated.

2. THE FIELD EXPERIMENT AND DATA PROCESSING

The site is located in south east of Tehran, in the eastern margin of Shahr-e-Rey. The hill is a

continuation of the Bibi Shahrbanoo Mountain toward the southern part of the city. This is a mound consisted of dolomite and limestone belonging to the Triassic and Cretaceous geological periods.

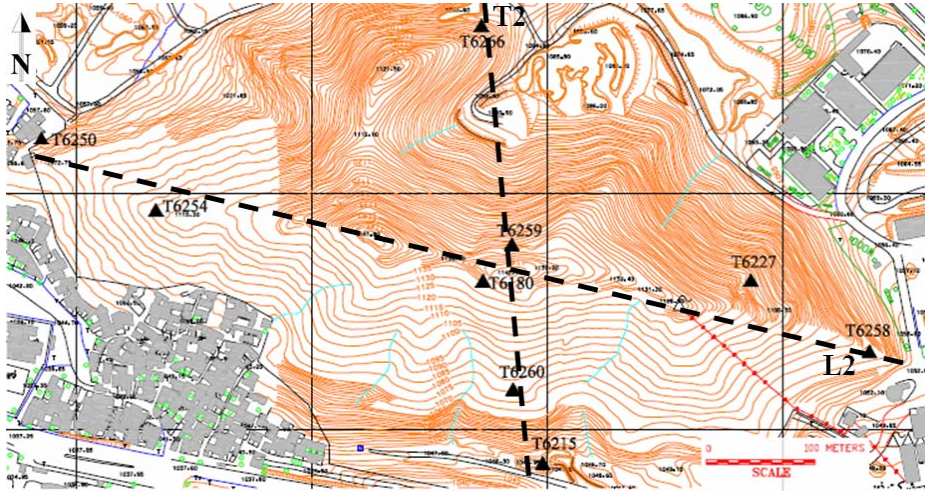


Figure 2.1. Topographic map of the site and location of temporary velocimetric network

The site was selected considering its homogeneity and absence of the soft soil layers. In this way we can assume that the variation of seismic motion is only due to topographic effect and not to the local weak layers. The average width of the hill is about 500-750 m. Nine seismic stations, as it is shown in Fig. 2.1, were installed across two longitudinal and transversal sections passing through the crest of the hill with the duration of about 4 days. The layout of the instrumentation was as follows; four stations were located at the base, four stations at mid-slope and one at the top of the studied hill. The broadband Guralp CMG-6TD was used, which is sensitive to ground vibration over a wide frequencies ranging 0.033-50 Hz. The sampling frequency was set as 100 Hz.

The horizontal to vertical spectral ratio technique, also called Nakamura's method (Nakamura 1989) or HVNR was used as a principal data processing procedure in order to extract the experimental transfer function of the site. The method relies on interpretation of Rayleigh waves in a single layer over half space. A further assumption is that vertical component of motion is not amplified by soft soil layer.

HVNR spectral ratios were calculated using the Geopsy software provided by the European SESAME consortium applying the following procedure. The continuously recorded data were split into 60 minutes microtremor records for the experiment. The mean and any linear trend were removed from the records. The records were band-passed filtered between 0.2-25 Hz. The stationary noise windows of 20 to 30 seconds were selected by the anti-triggering algorithm incorporated in the software with a 5% window overlapping. Then the squared average has been used to combine different horizontal spectra components. The Konno-Ohmachi smoothing function has been used to avoid spurious peaks or sharp troughs in the spectra. To minimize the border effects due to the windowing of the Fourier spectra, 5% cosine taper has been used. As the studied irregularity is relatively small, the source of the recorded microtremor assumed to be the same, so the spectral ratio between horizontal components of the stations located along the slope to the station installed at the foothill would be another choice to study the behavior of the hill. The method proposed first time in Borcherdt, 1970 using earthquake data. As the transversal section of the hill has just modeled, the results of the stations located along this section have been discussed here.

3. FIELD EXPERIMENT RESULTS

The experiment was carried out during 10th to 14th of March 2009. The continuous mode of recordings was selected to investigate local effects such as urban traffic and daily behaviour of HVNR

results. Despite of 4 days of recording due to malfunctions of battery only 17 hours of simultaneous records for all the stations could be used.

The continuous recordings were split into 60-minutes microtremor records. Each 60 minutes records which have been recorded by all stations were used for deriving HVNR curves. The results are presented in Fig. 3.1. Thin lines in this figure correspond to average of HVNR calculated for 60 minute microtremor segments and the thick line correspond to total average calculated for whole duration of measurement.

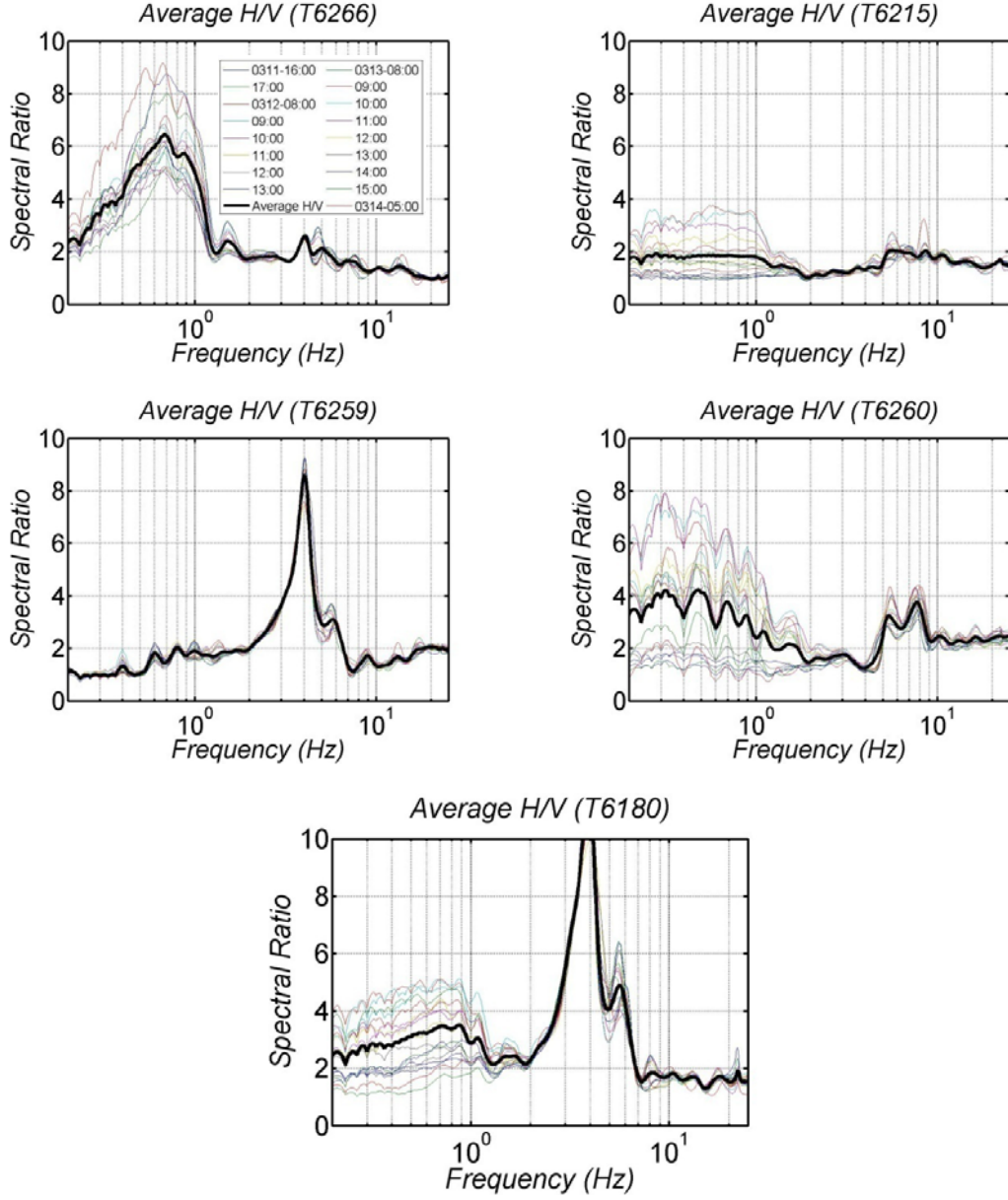


Figure 3.1. HVNR curves for the stations located on the transversal section of the hill

The results show relatively large scattering in low frequencies (less than 1 Hz) for stations T6260, T6266 and T6259, but the other curves show rather reliable results with little scattering. As it can be seen in Figure 5, a peak observed at frequencies around 4 Hz for almost all stations except station T6215 that is located at the hill-foot and experiences some sort of deamplification at this frequency

range. The HVNR values increases towards the hill-top and the maximum value can be observed at the crest (T6180 station). The spectral ratio is also significantly high for station T6259 at the same frequency as T6180 (4 Hz).

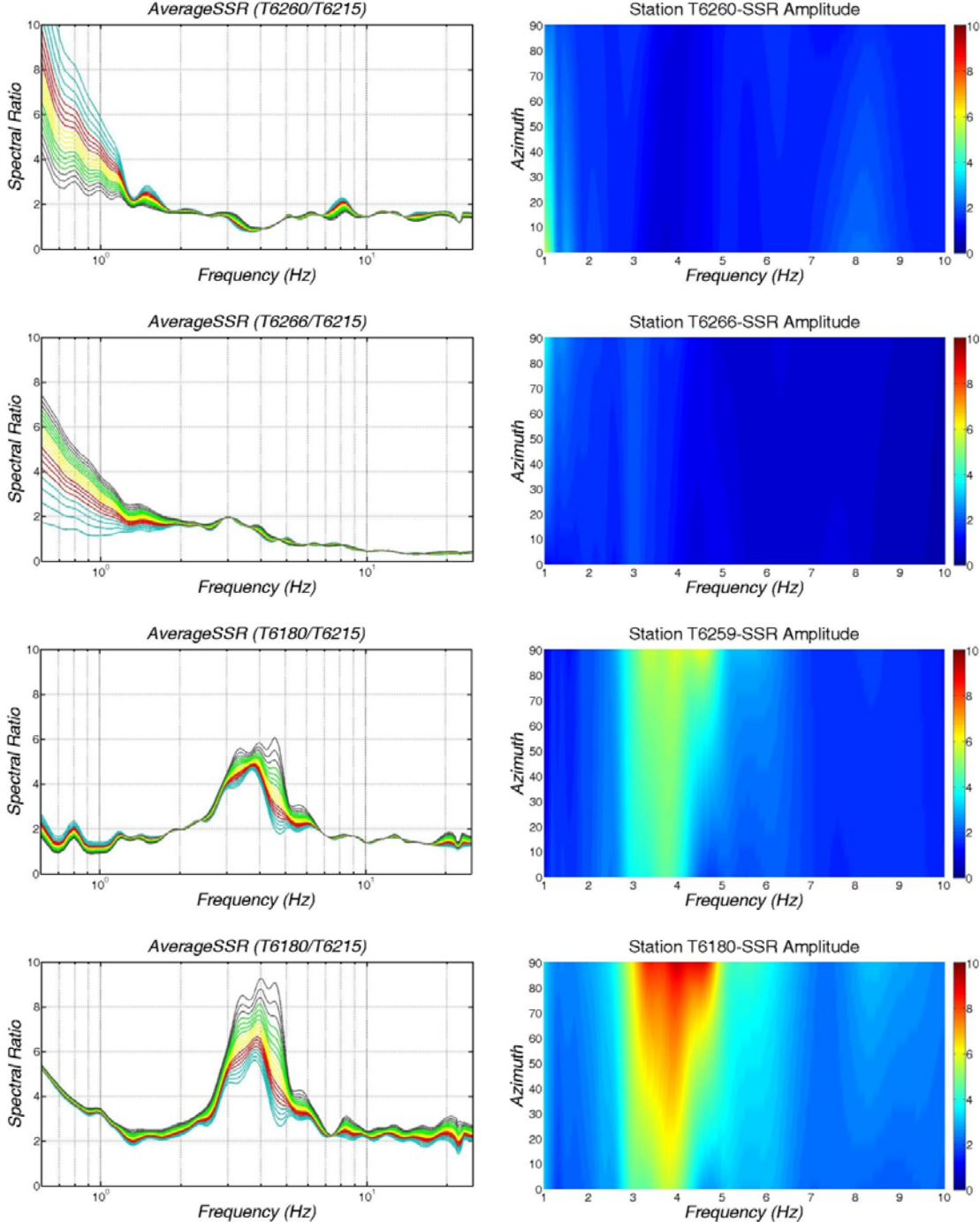


Figure 3.2. SSR curves for the stations located on the transversal section of the hill using station T6215 as the reference station

For SSR method the station T6215 has been selected as a reference station, based on its rather flat HVNR curve (Fig 3.2). The site/reference spectral ratios for South-Eastern Tehran experiment was

calculated for different stations located across the hill with respect to the station at base.

To investigate the differences between differently polarized horizontal components, directional spectral ratios were obtained by applying different rotation angles. In particular, for computing directional spectral ratios, the NS and EW components were rotated clockwise from the North, by between 0° and 90° , in angular steps of 5° , which provided for computation of 18 rotated components, which were representative of 18 directions of horizontal ground shaking.

As it is shown in Fig. 3.2. a clear peak is recognizable for station T6180, located at hill-top, at 4 Hz for different components that is identical to the peak derived from H/V curve shown in figure 5. The spectral ratio is lower than the amplification predicted by HVNR results. As it can be seen the curves show strong dependence of the amplification on the direction of microtremor recordings. The most significant site effect was obtained in the east-west direction.

The results for other station are also identical to HVNR results, especially for station T6259. A clear peak can be distinguished in both stations in accordance to their HVNR curves. The high amplitude in spectral ratio for low frequency range in some stations may be due to large scattering in spectra of the reference station T6215.

In order to have a better insight and better comparison between the spectral curves, spectral intensity concept has been used (Haghshenas et al. 2007). The spectral intensity using Eq. 3.1 determines the average amplitude of spectral ratios in a specific frequency range.

$$SI = \int_{f_{\min}}^{f_{\max}} A(f) df / f \quad (3.1)$$

In order to determine the area under the curve in each site, f_{\max} and f_{\min} supposed to be 10 and 1, respectively. The spectral intensity for the HVNR curves has been determined. As it is shown in Fig. 3.3., the maximum value corresponds to the station at the top, T6180. The SI value of other stations decreases gradually as the altitude of the station decreases.

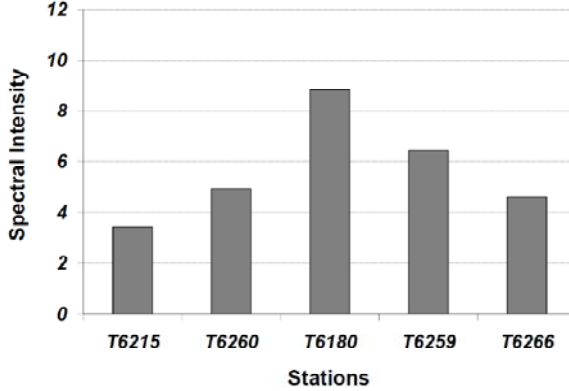


Figure 3.3. Spectral intensity of HVNR curves for the stations along the ridge

4. NUMERICAL MODLEING

The numerical simulations were executed using the well known time domain Boundary Element Method (BEM), based on 2D and 3D elastodynamics. The governing equation for an elastic, isotropic and homogeneous body, with a small amplitude displacement field, is:

$$(c_1^2 - c_2^2) \cdot u_{j,ij}(x,t) + c_2^2 \cdot u_{i,ij}(x,t) + b_i(x,t) - \ddot{u}(x,t)_i = 0 \quad (4.1)$$

Where c_1 and c_2 are the propagation velocities of the longitudinal and transverse waves respectively, u denote the displacement vector and b_i denotes the body force vector.

The term c_1 is given by

$$c_1^2 = (\lambda + 2\mu)/\rho \quad (4.2)$$

While the term c_2 is given by

$$c_2^2 = \mu/\rho \quad (4.3)$$

Where λ and μ are the Lame constants and ρ is the density. The corresponding governing boundary integral equation for an elastic, isotropic and homogeneous body can be obtained using the well known weighted residual method (Brennan and Dominguez, 1989), written as:

$$c_{ij}(\xi) \cdot u_i(\xi, t) = \int_{\Gamma} (G_{ij} * t_i(x, t) - F_{ij} * u_i(x, t)) d\Gamma \quad (4.4)$$

Where c_{ij} denotes the discontinuity term, resulting from the singularity of the F_{ij} fundamental solutions, u_i is the displacement vector, G_{ij} and F_{ij} are the transient displacement and traction fundamental solutions respectively. They represent displacements and tractions at a point x and at time t due to a unit point force applied at point ξ and at previous time $t = \tau$. The terms $G_{ij} * t_i$ and $F_{ij} * u_i$ are the Riemann convolution integrals and t_i represents the traction at the boundary. In the equation 4, the contributions due to the initial conditions and to the body forces are neglected. The implementation of the boundary integral equation needs approximation in both temporal and spatial variations of field variables. The detailed explanation of the method used in the code can be found in Kamalian et al. (2003). All 2D simulations performed by HYBRID code developed at IIEES by Kamalian et al. (2003).

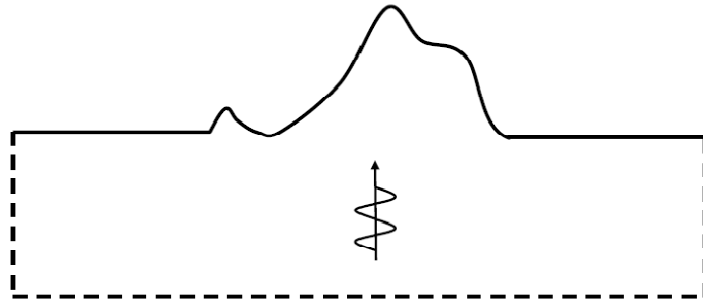


Figure 4.1. Schematic 2D discretization of generic ridge subjected to vertically propagating P-SV Ricker waves

Fig. 4.1 shows the schematic geometry and discretization of the studied hill subjected to vertically propagating SV and P waves of the Ricker type $f(t)$:

$$f(t) = [1 - 2 \cdot (\pi \cdot f_p(t - t_0))^2] \exp^{-(\pi \cdot f_p(t - t_0))^2} \quad (4.5)$$

In which f_p and t_0 denote the predominant frequency and appropriate time shift, respectively. The

boundary conditions of the problem were consisted of traction free ground surface and the seismic loading which was introduced by the Ricker wavelet as in Eqn. 4.5.

As the studied ridge located in proximity of a hill with the distance less than a three or four times of the hill dimension, it would be very interesting to study the effect of nearby topography on the response of the hill. In order to investigate the above effect, two profiles have been modelled, the first one, an isolated ridge without any nearby irregularities (S1 model) and the second one, a hill with nearby mountain (S2 model).

2D modelling has been carried out on two perpendicular sections, selected in a manner to pass near the installed stations. In this study, just the transverse model has been used. The model was subjected to vertically propagating SV and P waves of Ricker type. The boundary conditions are the same as the previous case study; traction free ground surface and the seismic loading which was introduced by the Ricker wavelet. Homogenous half space has a shear wave velocity of 1300 m/s and Poisson ratio of 0.33 and mass density of 2.4 t/m³. The information about the material properties comes from a seismic refraction test performed in the studied site. The Ricker wavelet, like previous part, has a predominant frequency of 3 Hz, time shift of 0.7s and amplitude of 0.001m.

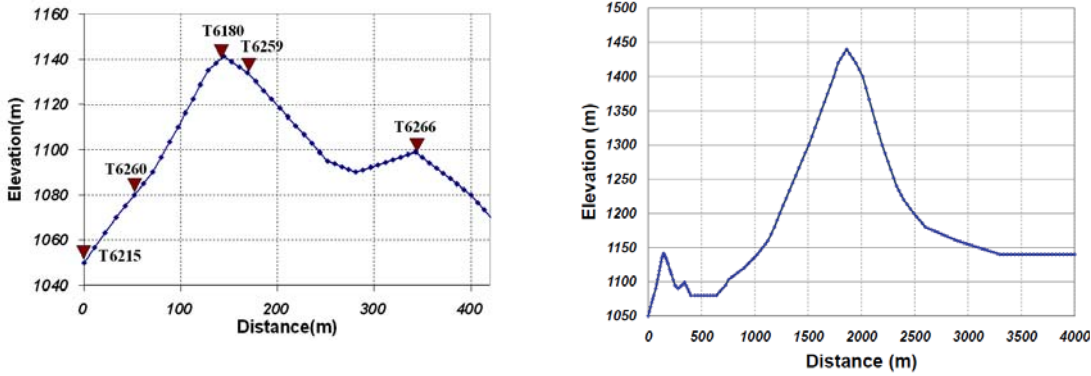


Figure 4.2. Left: Transversal section of the studied ridge with adjacent stations along the hill (S1 model), Right: The studied hill with its nearby topography

Fig. 4.2 (left panel) shows the transversal section (S1 model) with nearby station along the ridge. Fig.4.2 (right panel) depicts Bibi Shahrbanoo mount with the studied hill near to the mountain (S2 model).

4.1. Numerical Results: 2D Site Response

Both models were discretized using 499 nodes. The average spacing of the nodes in S1 model is 15m in the vicinity of the topography and 25m for S2 model. In both cases the model was characterized by 248 quadratic boundary elements. The half space, around the ridge, was discretized up to about eight times the profile length with a gradual increasing in elements dimension.

Fig.4.3 left, top panel depicts the time domain response for horizontal component for the profile S1 which has been subjected to a vertically propagating incident SV wave. The pattern of diffraction and refraction can be clearly seen. The maximum amplitude occurred at the top of the hill due to focusing of energy and interference between the incident and diffracted waves. Fig. 4.3 right, top panel shows the time domain response for horizontal component for S2 model subjected to vertically incident SV waves. The diffraction of waves due to complex geometry of the adjacent hills can be seen. The maximum amplitude occurred at the top of the higher hill and the studied hill experienced lower amplitude of diffracted waves. Fig.4.3 middle panels, show the location of different receiver points for the two models.

Fig. 4.3 left, bottom panel demonstrates the general pattern of amplification and deamplification of horizontal component for the studied hill (S1 model) subjected to vertically propagating SV Ricker wavelets. The amplification curve of the hill finds its maximum at the crest around frequencies 3-5 Hz and decays toward the bases. If the incident wave has a predominant frequency of smaller than the vibration frequency of the hill, decreasing the wave's frequency reduces the hill's effect on the ground response. In other words, if the hill is impinged by incident waves with wave lengths of much greater than that of the hill's width, which could occur in far field earthquakes and in rigid like media, the ground surface response would be approximately the same as the well known free field motion.

Fig. 4.3 right, bottom panel shows the general pattern of amplification and deamplification of horizontal component for the studied region and nearby irregularity (S2 model) subjected to vertically propagating SV wavelets. As it can be seen, the horizontal components of the motion, consists of sequential amplification and deamplification. Considering amplification pattern of the hill, at any point on the ground surface, irrespective of being on the hill or on the half-plane, the total motion differs from the free field motion (twice the incident motion). Moreover, for this section the interference of the amplification patterns would be also recognizable due to presence of nearby topography. The maximum amplification occurred at the crest of the higher hill because of its larger shape ratio, i.e. the ratio of height to effective width. The amplification of the studied hill, in this model, increased probably due to interference of waves diffracted from the nearby topography.

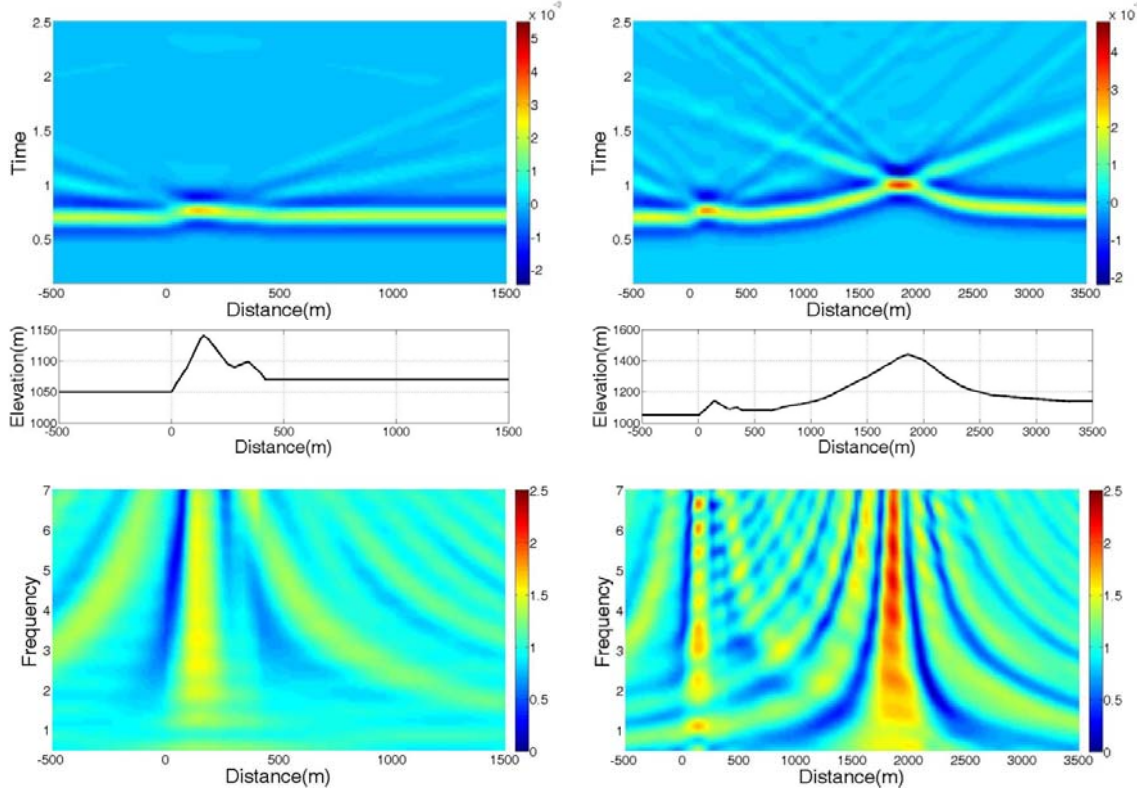


Figure 4.3. Left-top: Synthetic seismograms for horizontal component of motion for S1 model. Left-middle: Location of receiver points along S1 model. Left-bottom: Amplification pattern of horizontal component of motion. Right-top: Synthetic seismograms for horizontal component of motion for S2 model. Right-middle: Location of receiver points along S2 model. Right-bottom: Amplification pattern of horizontal component.

5. COMPARISON BETWEEN THE TWO DIFFERENT MODELS

In order to compare the numerical results with experimental ones, for both models transfer functions

were determined. For 2D configuration the frequency response at the surface of a topographic irregularity can be simply written as:

$$\begin{Bmatrix} O_1^k(f) \\ O_2^k(f) \end{Bmatrix} = \begin{bmatrix} H_{11}^k(f) & H_{12}^k(f) \\ H_{21}^k(f) & H_{22}^k(f) \end{bmatrix} \cdot \begin{Bmatrix} I_1(f) \\ I_2(f) \end{Bmatrix} \quad (5.1)$$

Where O_i^k denotes the i^{th} component of the ground motion at the point k of the model, I_i is the corresponding ground motion at the reference site, and H_{ij}^k is the frequency response of point k in the i^{th} direction due to an incident harmonic motion, with unit amplitude, oriented along j^{th} direction. For deriving 2D transfer function components, the time domain analysis will be limited to simply two independent P-SV analyses. In such analysis, we calculate four different transfer functions. For example, in order to determine $H_{21}^K(f)$, a time domain analysis is performed using the input motion oriented along x-axis, e.g. SV Ricker wave, then the Fourier transform of the response at K^{th} receiver point along y-axis ($O_2^k(f)$) would be determined, and the spectral ratio $H_{21}^K(f) = O_2^k(f)/I_1(f)$ would be easily calculated.

After determining the transfer function, the ratio of the H_{11} component of the receiver points corresponds to different stations along the studied ridge to the respective transfer function component of the receiver point located at the base of the ridge corresponds to the reference station was calculated. Fig. 5.1 depicts this ratio for different receiver points.

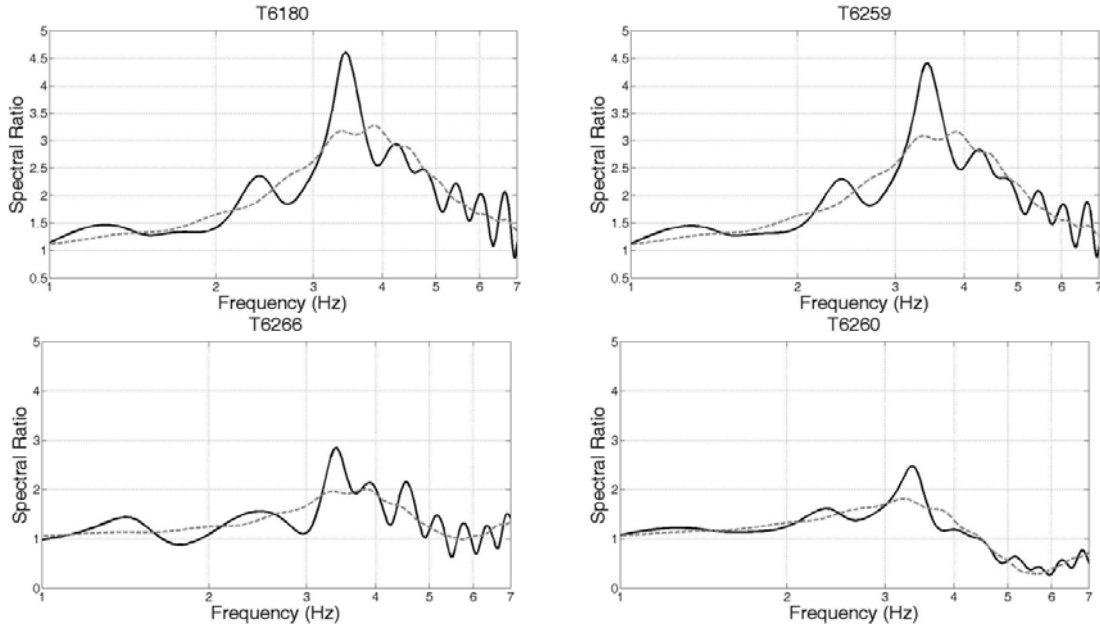


Figure 5.1. Comparison between the results of S1 and S2 model

As it can be seen, the general trend of the determined spectral ratios is almost the same. The frequency of vibration is around 3-4 Hz like experimental results. The spectral ratio determined from the S2 model is larger than the ones calculated from S1 model but the frequency content is nearly the same. The bumps observed in the curve may be due to diffracted waves of the modelled nearby topography.

6. CONCLUSIONS

In the current paper, the results of topography site effect using microtremor recordings and two

different ways of modelling presented. The predicted frequency of vibration from experimental studies for the site is between 4 and 5 Hz.

Moreover, the studied site was studied in two ways. In the first model, just the ridge has been modelled and the second one has been consisted of the studied hill and its nearby topography. Both sites have been excited with vertically propagating P-SV Ricker wavelet. Different transfer function components have been derived and amplification pattern of the hill determined for both models. Then the spectral ratio of the motions calculated at the top and the base of the hill has been compared.

As it is shown, the spectral ratios derived from numerical modelling are very similar in shape. They show the same frequency of vibration consistent with experimental results. But the spectral ratios determined in the model with nearby topography are closer to the real values derived from microtremor measurements. It seems that considering the effect of nearby irregularities can be helpful in estimating both frequency and amplification ratio of a ridge.

REFERENCES

- Bard P.Y. (1982). Diffracted waves and displacement fields over two-dimensional elevated topographies. *Geophysics Journal International* **71**, 731–760.
- Brebbia C.A. and Dominguez J. (1989). Boundary Elements, An Introductory Course. Computational Mechanics: Boston.
- Geli, L., Bard P.Y., Jullian B. (1988). The effects of topography on earthquake ground motion: a review and new results. *Bulletin of Seismological Society of America* **78**, 42-63.
- Graizer V. (2009). Low-velocity zone and topography as a source of site amplification effect on Tarzana hill, California. *Soil Dynamics and Earthquake Engineering* **29**, 324-332.
- Haghshenas, E., Bard, P.-Y., Theodulidis, N., (2007). Empirical evaluation of microtremor H/V spectral ratio. *Bulletin of Earthquake Engineering* **6**, 75-108.
- Kamalian M., Gatmiri B., Sohrabi-Bidar A. (2003). On Time-Domain Two-Dimensional Site Response Analysis of Topographic Structures by BEM. *Journal of Seismology and Earthquake Engineering* **5**, 35-45.
- Le Burn B., Hatzfeld D., Bard P.Y., Bouchon, M.(1999). Experimental study of the ground motion on a large scale topographic hill at Kitherion (Greece). *Journal of Seismology* **3**, 1-15.
- Nakamura Y. (1989). A method for dynamic characteristic estimation of subsurface using microtremor on the ground surface. *Quarterly Report of RTRI* **30**, 25-33.
- Rovelli A, Caserta A, Marra F, Ruggiero V. (2002). Can seismic waves be trapped inside an inactive fault zone? The case study of Nocera Umbra, central Italy. *Bulletin of Seismological Society of America* **92**, 2217–2232.